J Supercond Nov Magn (2013) 26:801–807
DOI 10.1007/s10948-012-2037-8

ORIGINAL PAPER

Epitaxial-Strain Effects on Electronic Structure and Magnetic Properties of Hexagonal $YMnO_3$ Thin Films Studied by Femtosecond Spectroscopy

K.H. Wu · H.-J. Chen · C.C. Hsieh · C.W. Luo · T.M. Uen · J.-Y. Lin · J.Y. Juang

Received: 4 November 2012 / Accepted: 1 December 2012 / Published online: 29 December 2012

Abstract In this paper, (001)-oriented hexagonal $YMnO_3$ (h-YMO) thin films with various nominal strain states were deposited on MgO(100), MgO(111), and YSZ(111) substrates by pulsed laser deposition. The in-plane orientation alignment and substrate-induced epitaxial strain between the h-YMO films and substrates are examined by X-ray diffraction (XRD) θ–2θ, Φ, and ω scans. The effects of epitaxial strain on the on-site Mn d–d transition energy $E_{dd}(T)$, and the Néel temperature (T_N) in these thin films are investigated by wavelength-tunable ultrafast pump-probe techniques. We find that the changes of $E_{dd}(T)$ and T_N depend on the type and magnitude of the epitaxial strain. The possible mechanisms for the observed strain effect on the electronic structure and associated magnetism are discussed.

Keywords Hexagonal $YMnO_3$ thin films · Strain effect · Crystalline structures · Temperature-dependent Mn d to d transition energy · Magnetization measurement

1 Introduction

The hexagonal multiferroic manganite (h-$RMnO_3$ (h-RMO)) is one of the most important families in multiferroic materials whose physical properties have been extensively studied both theoretically and experimentally, the study including the origins of ferroelectric ordering and antiferromagnetic (AFM) ordering, the microscopic mechanisms of the anomalous dielectric constant, blueshift of the Mn d to d transition energy (E_{dd}), and the magnetoelectric (ME) effect near the Néel temperature (T_N) [1–4]. In particular, through temperature-dependent high-resolution neutron scattering experiments, the ME coupling in this family of multiferroics was further identified to involve a significant magneto-elastic effect [4]. Therefore, the lattice strain induced by the magneto-elastic deformation is conceived to be the *dominant* factor giving rise the eventual ME coupling for this intriguing class of materials.

In fact, previously epitaxial strain resulted from the lattice mismatch between film and substrate has been demonstrated to significantly alter the physical properties in many materials [5–7] and, in some cases even were utilized to control the performance of devices made of these films. Recently, Singh et al. [8] reported that strained h-$YMnO_3$ (h-YMO) thin films on (0001) sapphire substrate with ZnGaO buffer layer exhibited an inverse S-shape anomaly in loss factor and T_N reduced from ∼70 K for bulk h-YMO to 30 K due to the strain. This indicates the possibility of tuning the multiferroic properties and raising T_N provided suitable strain states can be introduced in h-YMO thin films.

2 Sample Preparation

The pure phases of h-YMO films were deposited on MgO(100), MgO(111) and YSZ(111) substrates using pulsed laser deposition. A h-YMO single crystal, which was provided by Central Laboratory of Mineralogy and Crystallography at Bulgarian Academy of Sciences, was used for comparison. In order to optimize the deposition conditions, a KrF excimer laser was operated at the repetition

K.H. Wu (✉) · H.-J. Chen · C.C. Hsieh · C.W. Luo · T.M. Uen · J.Y. Juang
Department of Electrophysics, National Chiao Tung University, Hsinchu, Taiwan, ROC
e-mail: khwu@cc.nctu.edu.tw

J.-Y. Lin
Institute of Physics, National Chiao Tung University, Hsinchu, Taiwan, ROC

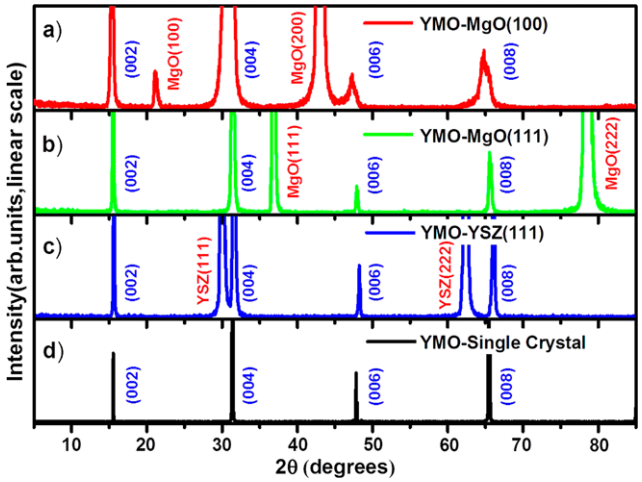

Fig. 1 The XRD θ–2θ patterns of the h-YMO thin films grown on (**a**) MgO(100), (**b**) MgO(111) and (**c**) YSZ(111) substrates, respectively. (**d**) The XRD θ–2θ pattern of the h-YMO single crystal

rate of 1–10 Hz with energy density of 2–5 J cm^{-2} and the substrate temperature (T_s) was varied between 700 and 880 °C with the oxygen partial pressure being controlled between background pressure (10^{-6} torr) and 0.3 torr during deposition. The optimum substrate temperatures and the oxygen partial pressures for depositing h-YMO films on MgO(100), MgO(100) and YSZ(111) substrates were 860, 860, 880 (°C), and 0.003, 0.3, 0.1 (torr), respectively. The film thicknesses, which were controlled by the number of laser pulses and confirmed by measurements carried out with an alpha step profilometer, were kept at ∼180 nm for all samples.

3 Strain Effects on the Characterizations of Samples

3.1 Crystalline Structures

X-ray diffraction (XRD) θ–2θ, Φ, and ω scans were used to examine the phase purity, crystallographic perfection, orientation relationship, and lattice constants of the h-YMO single crystal and films. Figure 1 shows the XRD θ–2θ patterns of all YMO samples. The results clearly indicate that all the samples are pure c-axis oriented h-YMO. The out-of-plane lattice constant c was calculated using Bragg's law for the position of (004) peak. In order to obtain the in-plane lattice constant (a (b)) and the atomic arrangement between the film and substrate, we used the four-circle X-ray diffractometer (Beamline 13A1 in National Synchrotron Radiation Research Center, NSRRC, Hsinchu, Taiwan) and performed the off-axis Φ-scan measurements. The typical results of h-YMO/MgO(100), h-YMO/MgO(111), and h-YMO/YSZ(111) films are shown in Fig. 2. It is evident that the in-plane orientation of the h-YMO/MgO(100) sample is of 12-fold symmetry as compared to the expected

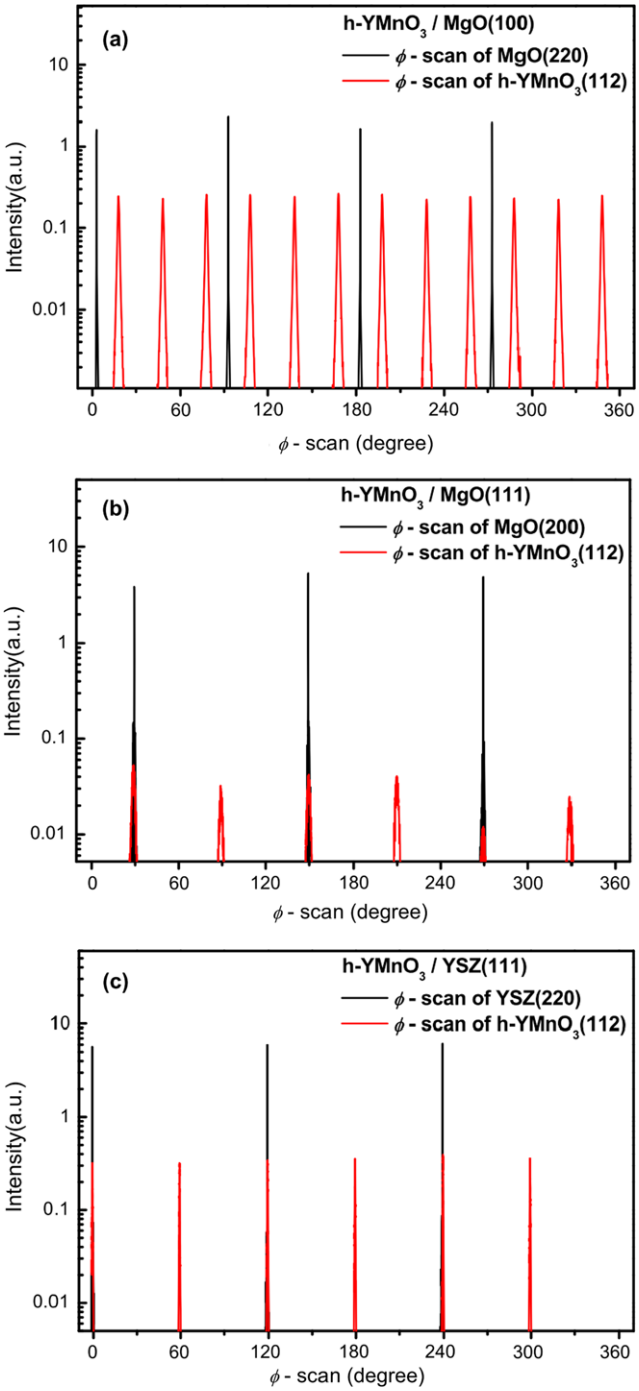

Fig. 2 The XRD Φ-scan patterns of the (**a**) h-YMO/MgO(100), (**b**) h-YMO/MgO(111), and (**c**) h-YMO/YSZ(111) thin films

6-fold symmetry exhibited in h-YMO/MgO(111) and h-YMO/YSZ(111) samples. Here, we explain the relative orientation between the h-YMO(001) film and YSZ(111) substrate as an example. In Fig. 3(a), a schematic drawing of the in-plane atomic arrangement between h-YMO thin film (right-hand side) and YSZ substrates (left-hand side) is shown. The left-hand side drawing shows the top view

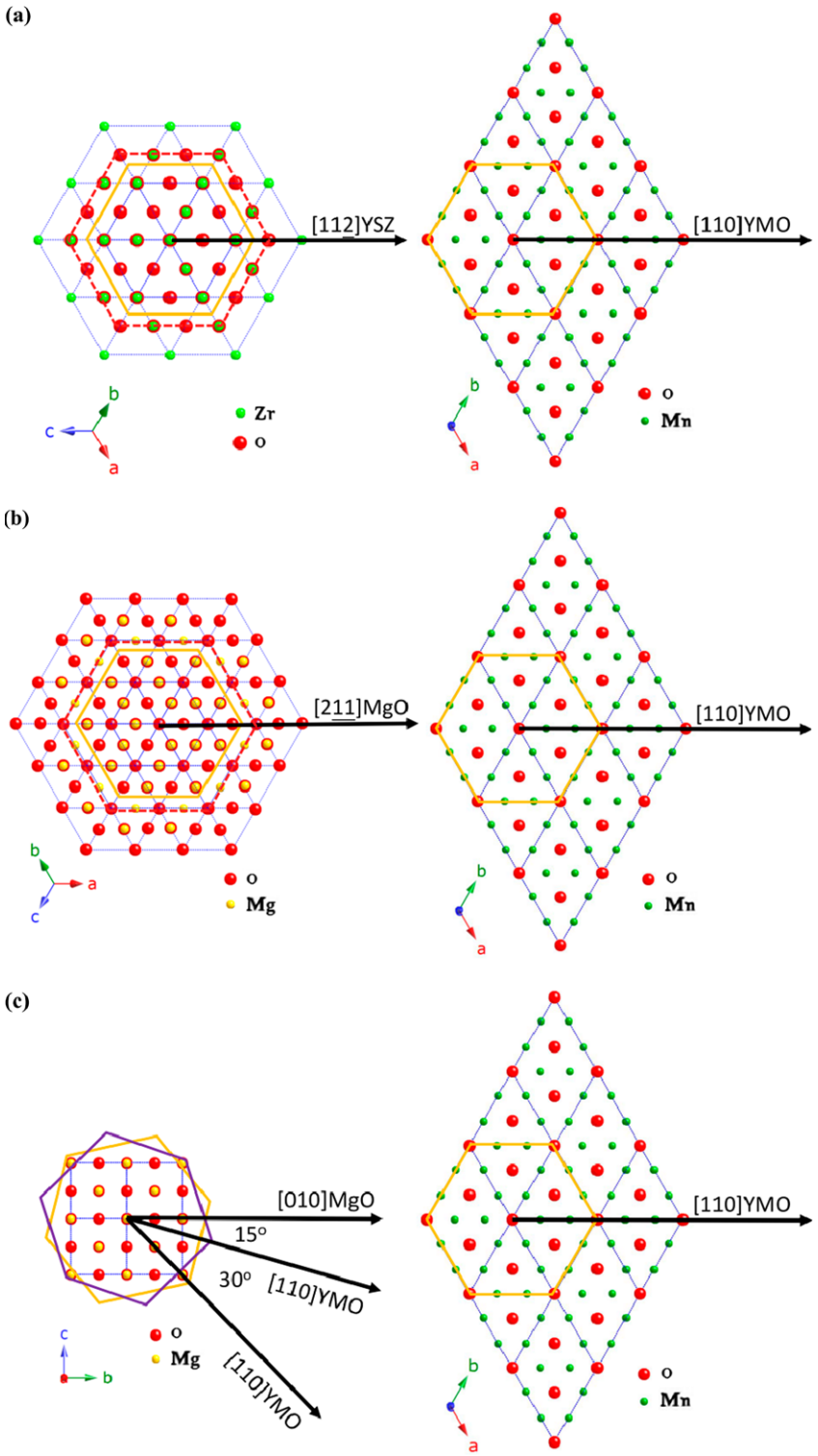

Fig. 3 The schematics show the in-plane atomic arrangements between the *h*-YMO(001) thin film and (**a**) YSZ(111) substrate, (**b**) MgO(111) substrate, (**c**) MgO(100) substrate

along the YSZ-[111] direction. The blue, red, and green balls indicate the sites of Y (or Zr), oxygen, and Mn ions, respectively. The right-hand side drawing shows a cross-section through the Mn ions, along the *ab* plane of *h*-YMO. The coincidence of the XRD Φ-scan off-normal YSZ(220) and *h*-YMO(112) peaks illustrates that YSZ[11$\underline{2}$] is parallel to *h*-YMO[110]. There is a similar symmetry for the *h*-YMO/MgO(111) case, but with MgO[2$\underline{11}$] parallel to *h*-YMO[110] direction (Fig. 3(b)). On the other hand, for the *h*-YMO grown on MgO(100) substrate, since the prin-

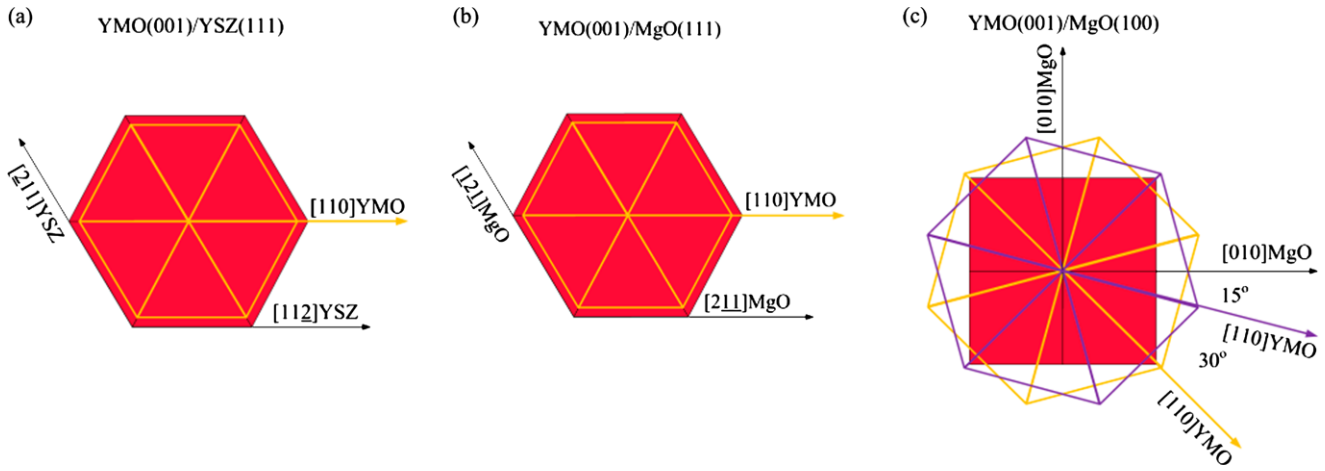

Fig. 4 A simplified schematic of the in-plane atomic arrangement for (**a**) *h*-YMO/YSZ(111), (**b**) *h*-YMO/MgO(111), and (**c**) *h*-YMO/MgO(100) films

Table 1 The lattice parameters and strain factors, E_{dd} (eV) at 250 K and T_N, for *h*-YMO/single crystal, *h*-YMO/MgO(100), *h*-YMO/MgO(111) and *h*-YMO/YSZ(111), respectively

	In plane lattice constant a (Å)	Out of plane lattice constant c (Å)	In plane lattice strain factor (%)	Out of plane lattice strain factor (%)	E_{dd} (eV) at 250 K	T_N (K)
YMO/Single Crystal	6.138	11.404	+0.00	+0.00	1.529	73
YMO/MgO(100)	6.120	11.440	−0.29	+0.32	1.522	63
YMO//MgO(111)	6.168	11.387	+0.49	−0.15	1.537	97
YMO/YSZ(111)	6.200	11.319	+1.01	−0.75	1.548	125

cipal crystallographic orientation of *h*-YMO can be aligned either along MgO[011] or MgO[0$\bar{1}$1] direction, the in-plane arrangements thus result in the observed 12-fold symmetry. The angle differences between MgO[010] and the two orientations of *h*-YMO[110] are 15° and 45°, respectively, as shown in Fig. 3(c). A simplified schematic of the in-plane atomic arrangement for these samples is summarized as shown in Fig. 4.

The strain factor is defined as $\varepsilon_d = \frac{d_{\text{film}} - d_{\text{bulk}}}{d_{\text{bulk}}}$, here d_{film} and d_{bulk} are lattice constants of respective crystallographic axis obtained from the present films. $\varepsilon_{a,b}$ and ε_c are the in-plane and out-of-plane strain factors, respectively. By comparing the lattice constants obtained from the single crystal and thin films grown on different substrates, one finds that the out-of-plane strain is tensile (+0.32 %) for *h*-YMO/MgO(100) thin film and compressive for *h*-YMO/MgO(111) (−0.15 %) and *h*-YMO/YSZ(111) (−0.75 %) thin films. On the other hand, the in-plane strain is compressive (−0.29 %) for *h*-YMO/MgO (100) thin film and tensile for *h*-YMO/MgO(111) (+0.49 %) and *h*-YMO/YSZ(111) (+1.01 %) thin films. The lattice constants and the strain factors along various orientations for various samples are listed in Table 1.

3.2 Electronic Structure and $E_{dd}(T)$

Recently, we have studied the ultrafast dynamics in *h*-Ho(Y, Yb)MnO_3 single crystals by the wavelength-tunable femtosecond optical pump-optical probe (OPOP) technique [9–11]. The temperature dependences of $E_{dd}(T)$, the anomalous blueshift near T_N, and how they are related to the magnetic ordering and the magnetization dynamics have been revealed in the experiment. The details of the OPOP experiment have been reported elsewhere [9–11] and only a brief description will be given here. The transient reflectivity change ($\Delta R/R$) curves for each sample (*h*-YMO/MgO(100), *h*-YMO single crystal, *h*-YMO/MgO(111), and *h*-YMO/YSZ(111)) were measured at various temperatures with wavelengths of the pump and probe beams being tuned at (a) 755 nm, (b) 770 nm, (c) 777 nm, (d) 785 nm, (e) 800, and (f) 815 nm.

As interpreted in [9], the amplitude of $\Delta R/R$ starts to drop steeply near a certain temperature and changes polarity at a lower temperature T_0, which means that the magnitude of the on-site Mn^{3+} d–d transition energy gap E_{dd} at this temperature is equal to the probe photon energy. In this way, by tuning the wavelengths of the probe beam, we can in principle obtain the temperature dependence of the energy gap $E_{dd}(T)$ for each sample, as shown in Fig. 5.

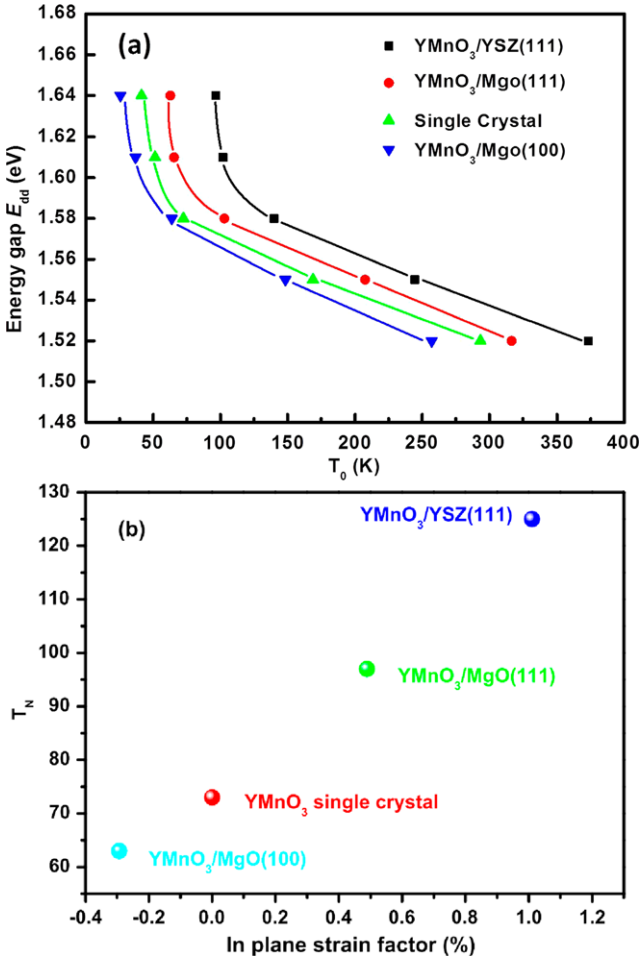

Fig. 5 The $E_{dd}(T)$ curves as a function of temperature T_0 (defined in the text). The temperature of the abruptly change in E_{dd} is defined as T_N. (**b**) The T_N versus in-plane strain factor for various h-YMO samples

For each E_{dd} curve displayed in Fig. 5, T_0 gradually shifts to lower temperatures with increasing photon energy indicates that E_{dd} exhibits a blueshift with decreasing temperature. T_N can be determined by locating the temperature where the E_{dd} value starts to increase abruptly. The extra enhancement in the blueshift of E_{dd} is believed to originate primarily from the emergence of the AFM superexchange interaction between the neighboring Mn^{3+} ions [2]. Figure 5 shows the results of $E_{dd}(T)$ as a function of temperature for various samples. It is interesting to find that while each $E_{dd}(T)$ curve has a similar anomalous blueshift behavior near T_N, the curves are shifted along the temperature axis for various samples. The possibility for the shift of $E_{dd}(T)$ curve and T_N appear to closely relate to the epitaxial strain induced in the thin films. The amount and direction of the shift depend on the magnitude and type of strain (compressive or tensile). If we choose the $E_{dd}(T)$ of the h-YMO single crystal to be a reference curve, then the $E_{dd}(T)$ curve of the h-YMO/MgO(100) films with tensile strain (+0.32 %) is evidently shifting to the left side. On the other hand, the $E_{dd}(T)$ curves of both h-YMO/MgO(111) and h-YMO/YSZ(111) films both with compressive strain (−0.15 % and −0.75 %, respectively) are clearly shifting to the right side. To further elucidate this behavior, we list the $E_{dd}(T)$ values of various samples at a temperature (∼250 K) in the spin disordering region (that is, a region of linear $E_{dd}(T)$) in Table 1. The E_{dd} value at $T = 250$ K decreases from 1.529 (E_{dd} of the single crystal) to 1.522 eV when the in-plane strain is compressive (−0.29 %). On the other hand, it increases from 1.529 to 1.548 eV when it reaches the tensile strain of 1.01 %. As is well known, in thin-film samples grown on heteroepitaxial substrates, a significant amount of stress is always present. Therefore, we speculate that the slight change in E_{dd} is due to the strain effect since the strain will induce the lattice distortion as well as change the lattice constants and, consequently, the electronic structure in h-RMO.

3.3 Magnetic Structure and Magnetization Measurement

The temperature-dependent magnetization (M–T curve) measurements were performed in a Quantum Design SQUID magnetometer by applying a small external field (100–500 Oe) either parallel or perpendicular to the c-axis. Both the zero field cool (ZFC) and field cool (FC) schemes were measured.

Figure 6(a) shows the M–T curve of the h-YMO single crystal. The $T_N = 75$ K at the formation of AFM long range is apparently observed. This result is similar to those results reported in [12, 13]. However, as shown in Figs. 6(b)–(d), the M–T curve obtained from the thin-film samples is significantly different from that obtained from the single crystal. In some cases, a small second phase transition, which may due to a superspin-glass-like (SSG) transition associated with disorder-coupled spin reorientation behavior [12, 14], was also observed at a lower temperature, which is called the temperature of spin reorientation T_{SR} ($T_{SR} \sim 40$ K in h-YMO/YSZ(111) sample and ∼28 K in h-YMO/MgO(100) sample). As pointed out by Sharma et al. [12] for geometrically frustrated systems such as YMO the ground state magnetic structure remains as highly degenerate low lying states even below T_N. Thus, in single crystals the intrinsic spin reorientation of Mn moments occurring around T_{SR} is barely discernible in the M–T measurements. This degeneracy, however, might be easily lifted by the disorders existent in the polycrystalline powders or films, resulting in short range weak ferromagnetism and the SSG behavior manifested in M–T measurements. To further delineate the scenario of SSG and to clarify that there indeed exists weak ferromagnetism below the spin reorientation temperature, we measured the field dependent magnetization behavior (M–H curve) at various temperatures with

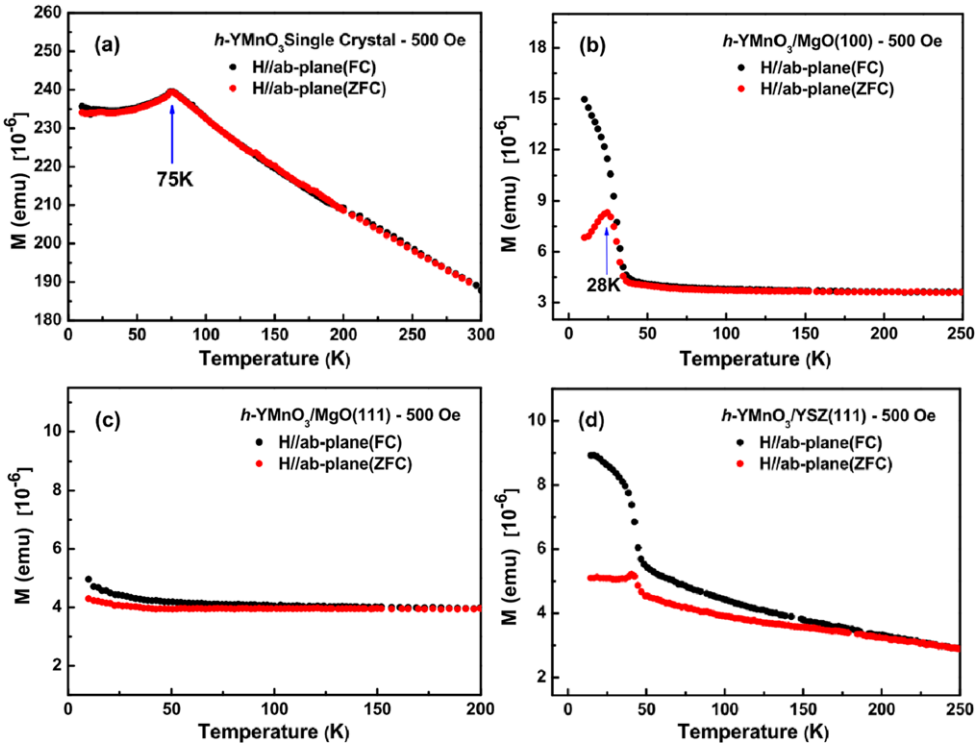

Fig. 6 Some typical M–T curves for (**a**) h-YMO single crystal, (**b**) h-YMO/MgO(100), (**c**) h-YMO/MgO(111), and (**d**) h-YMO/YSZ(111) thin films, respectively

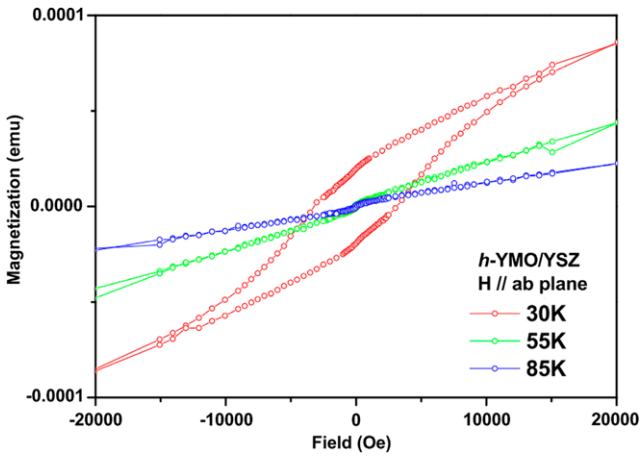

Fig. 7 The field dependent magnetization behavior of the h-YMO(00l)/YSZ(111) thin film measured at several temperatures. Notice the hysteresis loop appearing at 30 K, indicating the existence of SSG characteristics

the applied field in the a–b plane in the range of −7 T–7 T. As shown in Fig. 7, the M–H curves are apparently linear at 85 K and 55 K. However, an apparent hysteresis typical for weak ferromagnetism spin-glass system is evident at $T \sim 30$ K. In contrast, when the temperature is above 40 K, although the system is in AFM state, there is no hysteresis in M–H curves observed [14].

In fact, T_N in the M–T curve obtained from thin films is difficult to identity and usually is defined the point where the ZFC M–T curve deviates from the FC one [15–17]. On the other hand, one advantage of using the ultrafast OPOP spectroscopy to study the ultrafast dynamics in manganites is that the temperature dependence of the relaxation behavior (magnitude, relaxation time and coherent phonon oscillation) always exhibits a dramatic change near the transition temperature (T_c or T_N), which may reveal the valuable information about the physical mechanisms governing the intriguing properties of these materials. Therefore, it is a sensitive tool to monitor the transition temperature of these materials. As explained above, for each E_{dd} curve displayed in Fig. 5(a), the T_N can be determined by locating the temperature where the E_{dd} value starts to increase abruptly. In this way, the T_N values are estimated to be 63, 73, 97, and 125 K for h-YMO/MgO(100), h-YMO single crystal, h-YMO/MgO(111), and h-YMO/YSZ(111) samples, respectively.

It is reasonable to conjecture that the great enhancement of T_N may also relate to the epitaxial strain of the samples and the scenario of the ME control described in the present work: For the hexagonal multiferroic manganite, a strong spin-lattice coupling in h-RMO have been revealed by the anomalies of the thermal expansion coefficients along the a and c axes [1]. The neutron diffraction experiments also have exhibited the giant magneto-elastic coupling, effective magnetic moment per site, and large variations in lattice parameters, Mn–O bond lengths, and O–Mn–O bond angles near T_N [4]. The tremendous alternations of crystalline structure near T_N will then induce a change in the electric dipole moments and dielectric anomaly. We may pro-

pose that the existence of the epitaxial strain in thin films changes the lattice constants and distorts the lattice structure, and then further modifies the above physical properties. Especially, it may change Mn–O lengths, O–Mn–O bond angles, and Mn–O–Mn superexchange interaction in the ab plane and thus the temperature for AFM ordering. The lattice distortion due to the epitaxial strain may also affect the magneto-elastic coupling and consequently the ferroelectric polarization. Therefore, it is possible to control the ME effect of h-RMO by the lattice strain.

4 Conclusions

In summary, we prepared pure (001)-oriented h-YMO thin films with either tensile or compressive strain by pulsed laser deposition. The in-plane orientation alignment and substrate-induced epitaxial strain between the h-YMO films and substrates are delineated in detail. The effect of strain on the magnitude of E_{dd} and the temperature of magnetic transition are revealed in the OPOP experiment. We found that while the E_{dd} shifts slightly, however, T_{N} exhibited a significant shift and the direction of shift depends on the strain type. The existence of the epitaxial strain may change the lattice constants and distort the lattice structure then further modify the electric, magnetic and multiferroic properties in these materials.

Acknowledgements This project is financially sponsored by the National Science Council (grant no. NSC 98-2112-M-009-006-MY3) and the Ministry of Education (2010 MOE ATU program at NCTU) of Taiwan, R.O.C.

References

1. Lorenz, B., Wang, Y.Q., Sun, Y.Y., Chu, C.W.: Phys. Rev. B **70**, 212412 (2004)
2. Souchkov, A.B., Simpson, J.R., Quijada, M., Ishibashi, H., Hur, N., Ahn, J.S., Cheong, S.W., Millis, A.J., Drew, H.D.: Phys. Rev. Lett. **91**, 027203 (2003)
3. Choi, W.S., Moon, S.J., Seo, S.S.A., Lee, D., Lee, J.H., Murugavel, P., Noh, T.W.: Phys. Rev. B **78**, 054440 (2008)
4. Lee, S., Pirogov, A., Kang, M., Jang, K.-H., Yonemura, M., Kamiyama, T., Cheong, S.-W., Gozzo, F., Shin, N., Kimura, H., Noda, Y., Park, J.-G.: Nature **451**, 805 (2008)
5. Yeh, N.-C., Fu, C.-C., Wei, J.Y.T., Vasquez, R.P., Huynh, J., Maurer, S.M., Beach, G., Beam, D.A.: J. Appl. Phys. **81**, 8 (1997)
6. Choi, K.J., Biegalski, M., Li, Y.L., Sharan, A., Schubert, J., Uecker, R., Reiche, P., Chen, Y.B., Pan, X.Q., Gopalan, V., Chen, L.-Q., Schlom, D.G., Eom, C.B.: Science **306**, 1005 (2004)
7. Haeni, J.H., Irvin, P., Chang, W., Uecker, R., Reiche, P., Li, Y.L., Choudhury, S., Tian, W., Hawley, M.E., Craigo, B., Tagantsev, A.K., Pan, X.Q., Streiffer, S.K., Chen, L.Q., Kirchoefer, S.W., Levy, J., Schlom, D.G.: Nature (London) **430**, 758 (2004)
8. Singh, A.K., Snure, M., Tiwari, A., Patnaik, S.: J. Appl. Phys. **106**, 014109 (2009)
9. Shih, H.C., Lin, T.H., Luo, C.W., Lin, J.-Y., Uen, T.M., Juang, J.Y., Wu, K.H., Lee, J.M., Chen, J.M., Kobayashi, T.: Phys. Rev. B **80**, 024427 (2009)
10. Shih, H.C., Chen, L.Y., Luo, C.W., Wu, K.H., Lin, J.-Y., Juang, J.Y., Uen, T.M., Lee, J.M., Chen, J.M., Kobayashi, T.: New J. Phys. **13**, 053003 (2011)
11. Wu, K.H., Chen, H.J., Chen, Y.T., Hsieh, C.C., Luo, C.W., Uen, T.M., Juang, J.Y., Lin, J.-Y., Kobayashi, T., Gospodinov, M.: Europhys. Lett. **94**, 27006 (2011)
12. Sharma, P.A., Ahn, J.S., Hur, N., Park, S., Kim, S.B., Lee, S., Park, J.-G., Guha, S., Cheong, S.-W.: Phys. Rev. Lett. **93**, 177202 (2004)
13. Katsufuji, T., Mori, S., Masaki, M., Moritomo, Y., Yamamoto, N., Takagi, H.: Phys. Rev. B **64**, 104419 (2001)
14. Hsieh, C.C.: Ph.D. dissertation, National Chiao Tung University, Hsinchu, Taiwan, ROC (2008)
15. Veres, A., Noudem, J.G., Fourrez, S., Bailleul, G.: Solid State Sci. **8**, 137 (2006)
16. Posadas, A., Yau, J.-B., Ahn, C.H.: Phys. Status Solidi (b) **243**, 2085 (2006)
17. Marti, X., Skumryev, V., Ferrater, C., García-Cuenca, M.V., Varela, M., Sánchez, F., Fontcuberta, J.: Appl. Phys. Lett. **96**, 222505 (2010)